PIER B

Design and Development of Four Port Wideband High Isolation Koch Curve Fractal MIMO Antenna

Ashwini Kumar[1], Basudha Dewan[1], Amit K. Jain[1], Pratish Rawat[1],
Zahriladha Zakaria[2], and Ahmed J. A. Al-Gburi[2, *]

[1]*Faculty of Engineering and Technology, Poornima University, Jaipur, Rajasthan 303905, India*
[2]*Centre for Telecommunication Research & Innovation (CeTRI)*
Fakulti Teknologi dan Kejuruteraan Elektronik dan Komputer (FTKEK)
Universiti Teknikal Malaysia Melaka (UTeM), Malacca, Malaysia

ABSTRACT: An innovative four-port Coplanar Waveguide (CPW) Multi-Input Multi-Output Antenna (MIMOA) based on a Koch Curve Fractal (KCF) with high isolation is proposed in this article. The High Frequency Structure Simulator (HFSS) is used for performance analysis and parametric optimization. Initially, a KCF-based CPW-fed single-element patch antenna is designed, which is later transformed into a four-port MIMOA (FPMIMOA). The proposed MIMOA is fabricated on an FR4 substrate and offers a wide impedance bandwidth of 1.23 GHz (4.46–5.69 GHz), centered at 4.92 GHz. It exhibits excellent diversity performance, including a Channel Capacity Loss (CCL) of less than 0.4 bits/s/Hz, an Envelope Correlation Coefficient (ECC) below 0.004, a Diversity Gain (DG) greater than 9.8, a Mean Effective Gain (MEG) below 3 dB, and a Total Active Reflection Coefficient (TARC) less than -20 dB from Port 1 to the other ports. It also demonstrates an isolation level of 28 dB across the operating band. Furthermore, the proposed MIMOA achieves a high radiation efficiency (η) of 94% and a gain of 3.14 dBi. The antenna has been fabricated and experimentally tested to validate the simulated results. This MIMOA is suitable for applications such as public safety, the 5G sub-6 GHz band (4.8–5.0 GHz), and the 5.2 GHz Wireless LAN (5.15–5.35 GHz).

1. INTRODUCTION

Demand of high data rate and low Channel Capacity Loss (CCL) in the field of modern communication steers the research towards MIMO systems working at specific frequencies [1, 2]. MIMO configured antennas provide high data rate with low CCL which is a key requirement of next generation communication systems [3–5]. MIMOA configuration uses many antennas at both receiving and transmitting sides which helps in improving channel capacity without the use of extra power and bandwidth [3]. However, designing a compact MIMOA configuration is challenging as designers have to maintain high isolation and η [4]. Antenna designers have to take care the isolation in MIMOA design to fulfill the requirement of channel capacity [5].

Many approaches have been explored in prior research to mitigate mutual coupling in MIMO antenna systems. A particular study [6] examined the design of a MIMOA that has two elements, incorporating an inverted T- and E-shaped element. For improving isolation, a parasitic resonator was used in the design. However, isolation was improved up to a limited extent of 20 dB. A MIMOA with four elements is proposed in [7], which uses a rectangular split ring resonator and modified Z-shaped slot for improving isolation.

A different study [8] introduced a small size MIMOA design that incorporated four elements arranged orthogonally, along with a split ring resonator embedded in the antenna radiator. Although the isolation of 14 dB was achieved, it was below the required level for MIMOA system. Further exploration of techniques involved the utilization of two rectangular microstrip lines and a defective ground plane [9]. Additionally, a dual-band MIMO Antenna design incorporating L-shaped split-ring resonator loaded monopole elements was also investigated [10]. However, both of these approaches encountered limitations in terms of the achieved isolation and compactness. A four-element MIMOA incorporating a decoupling line is reported in [11]. A 30 dB isolation was achieved successfully, by utilizing two cross decoupling lines. In [1], a MIMOA with a semi-circular cut on a corner and defected ground was proposed
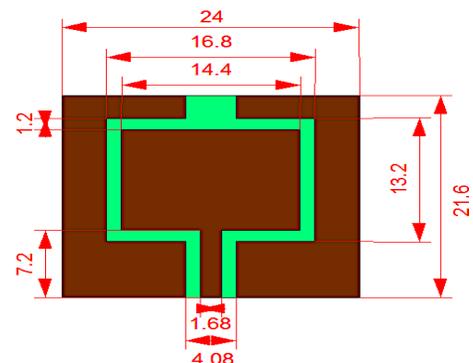

FIGURE 1. CPWRPA design with dimensional details in mm.

* Corresponding author: Ahmed Jamal Abdullah Al-Gburi (Ahmedjamal@ ieee.org, ahmedjamal@utem.edu.my).
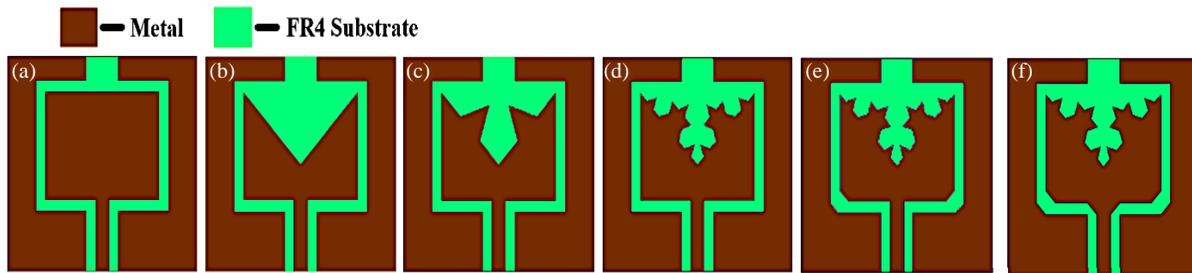
15

FIGURE 2. Transformation from initial to final stage, (a) CPWRPA, (b) 1st iteration KCF, (c) 2nd iteration KCF, (d) 3rd iteration KCF, (e) 3rd iteration KCF with patch chamfered, and (f) SEKCFA design.

for the 5G and 6G bands. In this design, a special structure in connected ground was used for improving the isolation. In [2], a two-port MIMOA was proposed with a multilayer structure for multiband applications which was designed on an FR4 substrate having an isolation of 15 dB. In [12], a MIMOA was proposed with two and four port layouts which has a bandwidth of 320 MHz with an isolation of 20 dB.

Two studies investigating 1×2 and 2×2 MIMOA systems [13, 14] found that isolation could be improved simply by rotating the unit element, eliminating the requirement of additional decoupling method. In [15], T- and π-shaped strips were employed for enhancing isolation. Other approaches for decoupling discussed in the literature involve metamaterials, short-neutral lines, ground with defects, and self decoupling mechanisms [16–20]. These methods have been developed for improving the isolation in compact MIMOA systems and to offer potential solutions to enhance overall performance.

In this article, an innovative four-port CPW MIMO antenna based on a Koch Curve Fractal (KCF) with high isolation is proposed, operating at 4.92 GHz. The proposed MIMO antenna (MIMOA) exhibits low Envelope Correlation Coefficient (ECC), low Channel Capacity Loss (CCL), high radiation efficiency (η), and high gain, making it suitable for achieving high data rates and large channel capacity. The antenna consists of CPW-fed KCF radiating elements. A parametric analysis is conducted to determine the optimal dimensions of the MIMO Koch curve fractal antenna, and various configurations are evaluated to improve isolation. The proposed MIMOA is applicable to public safety communications, 5G sub-6 GHz applications (4.8–5.0 GHz), and Wireless LAN (5.15–5.35 GHz).

The major contributions of this work are as follows:

- The proposed MIMOA achieves a wide bandwidth of 1.23 GHz (from 4.46 to 5.69 GHz) with minimal design complexity compared to [21–24].

- The four-element MIMOA has compact dimensions of $0.7\lambda \times 0.75\lambda$ (where λ is the wavelength at 4.46 GHz), which is smaller than those in [21, 23–26].

- The proposed MIMOA achieves a gain of 3.14 dBi, higher than those reported in [8, 25, 27], and a radiation efficiency of 94%.

- The antenna demonstrates superior isolation and diversity performance compared to [8, 13, 14, 21–23, 26, 27], making it highly suitable for multipath environments.

2. ANTENNA DESIGN

This section outlines the progression of antenna design, starting from a CPW-fed Rectangular Patch Antenna (CPWRPA) to a Single Element KCF Antenna (SEKCFA), and further evolving into Two Port MIMOA (TPMIMOA) and FPMIMOA (FPMIMOA) layouts.

2.1. CPW Fed Rectangular Patch Antenna (CPWRPA) to Single Element KCF Antenna (SEKCFA) Design

Antenna designers and researchers used fractal structures to achieve compactness, wider operating bandwidth, and multi-frequency operation in antennas [28–30]. In this work, KCF is used to attain wider bandwidth. Figure 1 shows the CPWRPA design at initial phase with the dimensional details of the design in millimeters. After designing CPWRPA the structure is transformed into SEKCFA by integrating KCF on the top side of CPWRPA as shown in Figure 2 from image (a) to (f). The S_{11} of all stages of design from CPWRPA to SEKCFA are shown in Figure 3. The SEKCFA operates within a frequency range of 4.46 to 5.69 GHz, offering a bandwidth of 1.23 GHz. In contrast, the CPWRPA covers only a small range from 4.50 to 4.73 GHz, resulting in a bandwidth of 0.23 GHz. The performance of the design from initial to final stage got improved in terms of S_{11} which can be analyzed form Figure 3.
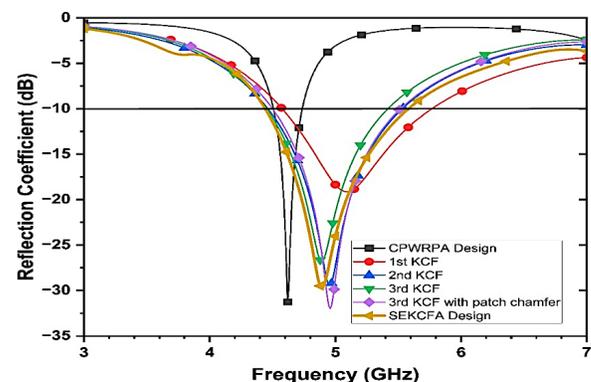

FIGURE 3. S_{11} of CPWRPA and SEKCFA design.

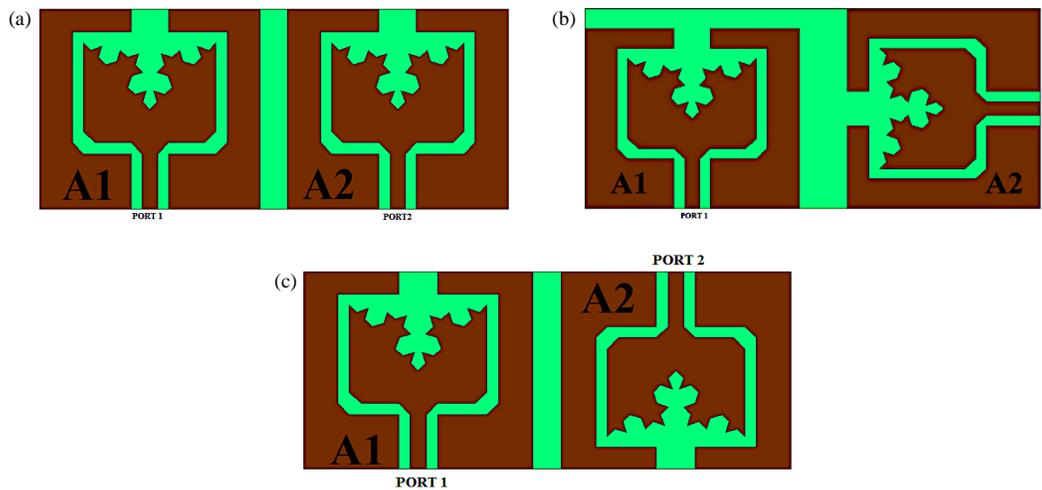**FIGURE 4**. TPMIMOA. (a) Layout 1: $0°$ orientations of A2 element, (b) Layout 2: $90°$ orientations of A2 element, (c) Layout 3: $180°$ orientations of A2 element.

KCF integration in the CPWRPA influences the Surface Current (SC) distribution, effectively increasing the path length of the current along the surface of antenna which results in the bandwidth enhancement. A comparison of the bandwidths is shown in Figure 3 between the CPWRPA and SEKCFA, which confirm the improvement in bandwidth.

2.2. TPMIMOA Layout

SEKCFA has been utilized to design the TPMIMOA after carefully analyzing the results of SEKCFA in terms of S_{11}. The improvement in S_{11} of the initial design as CPWRPA to SEKCFA can be analyzed from Figure 3, where it can be noticed that the Bandwidth (BW) gets improved significantly. TPMIMOA Layout has been designed using SEKCFA on an FR4 substrate (Dielectric constant — 4.4 and loss tangent — 0.02) having size of $51 \times 21.6 \times 1.6\,\text{mm}^3$ as shown in image (a) of Figure 4. The S-parameters (S-P) of this layout can be seen in Figure 5(a). For further examining the TPMIMOA performance, the orientation of A2 element has been varied as shown in images (b) and (c) of Figure 4. The S-P of other two layouts have been analyzed, shown in images (b) and (c) of Figure 5. From Figure 5 it can be seen that the overall performance of TPMIMOA with a $90°$ orientation compared to A1, i.e., Layout 2, exhibits a notable improvement in isolation, reaching $-30\,\text{dB}$. The performance of Layout 2 with $90°$ orientation of A2 is better than the other two layouts. SC distribution over the surface of antenna in Layout 2 can be visualized in Figure 6 at $4.92\,\text{GHz}$. Although the S_{22} in Layout 2 has been shifted a little, it does not affect the antenna performance for the targeted applications as it covers the required band.

Figure 6(a) shows the SC distribution when Port 1 is excited, while the other is kept at matched state, and Figure 6(b) shows the vice-versa condition in which Port 2 is excited, while the other is kept at matched state. When Port 1 is excited, the SC density is more over the A1 surface, and similarly when Port 2 is excited the SC density is higher at A2 surface. Moreover, Figure 6 illustrates a fascinating phenomenon: a reverse current

flows across the surfaces of A1 and A2. This reverse current effectively inhibits the current from moving toward the adjacent element, thereby enhancing isolation.

2.3. Three Port MIMO Antenna (THPMIMOA) Layout

THPMIMOA Layout as shown in Figure 7 is designed after TPMIMOA. It is designed on a hexagon-shaped substrate that has a side length of $35\,\text{mm}$ and height of $1.6\,\text{mm}$. The S-P of this layout is shown in Figure 8 which clearly indicates an excellent isolation of more than $25\,\text{dB}$.

Figure 9(a) shows the SC distribution when Port 1 is excited, while the other two are kept at matched state; Figure 9(b) shows the condition in which Port 2 is excited, while the other two are kept at matched state; Figure 9(c) shows the condition in which Port 3 is excited, while the other two are kept at matched state. When a port is excited, the SC density is more over the excited antenna. Diversity performance parameters like: ECC, DG, MEG, and TARC of the THMIMOA are analyzed. Envelope Correlation Coefficient (ECC) < 0.002, Diversity gain (DG) > 9.9, MEG $< -3\,\text{dB}$, Total Active Refection Coefficient (TARC) $\approx -30\,\text{dB}$ from Port 1 to other ports, and isolation of $25\,\text{dB}$ across the band. THMIMOA offers high radiation efficiency (η) of 93% and gain of $1.8\,\text{dBi}$. Figures 10 to 14 illustrate the aforementioned parameters in graphical form.

2.4. FPMIMOA Layout

The results of TPMIMOA (Layout 2) are very promising, leading to the development of the FPMEMA layout as an extended version of TPMIMO (Layout 2), as shown in Figure 15. FPMIMO has a volume of $51 \times 51 \times 1.6\,\text{mm}^3$. Figure 16 shows S-P of the FPMIMOA layout, clearly indicates an excellent isolation of nearly $28\,\text{dB}$. Figure 17 illustrates the SC density over A1, A2, A3, A4 (SEKCFA elements) at $4.92\,\text{GHz}$. Figure 17 demonstrates that the excited antenna element exhibits a higher current density on its surface, whereas the other radiating elements display relatively lower current density levels. Fig-
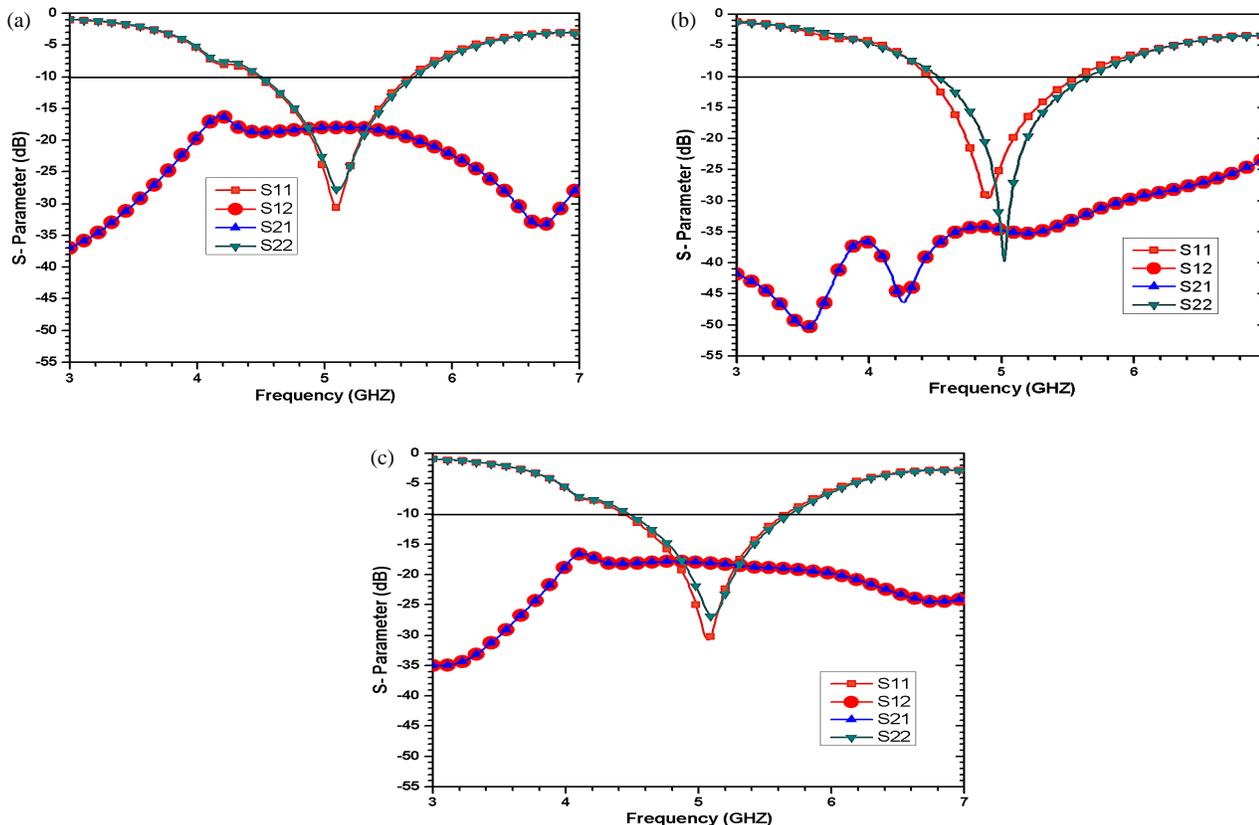
FIGURE 5. S-P of TPMIMOA. (a) Layout 1: 0° orientations of A2 element, (b) Layout 2: 90° orientations of A2 element, (c) Layout 3: 180° orientations of A2 element.
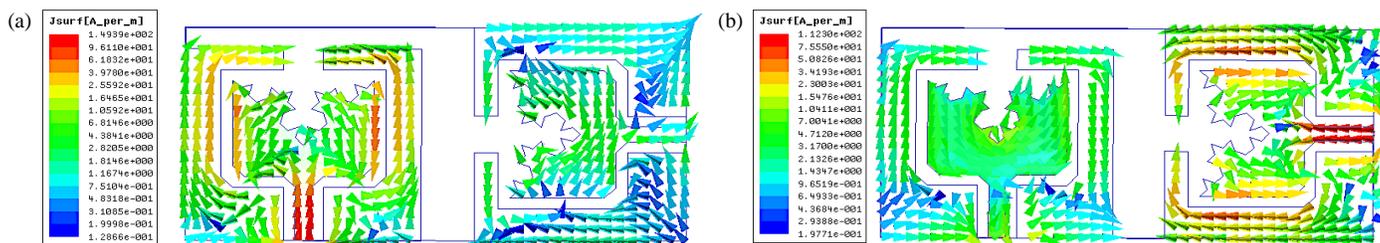

FIGURE 6. SC distributions over the antenna surface in Layout 2 at 4.9 GHz when (a) Port 1 is excited while the other remains in a matched state, and (b) Port 2 is excited while the other remains in a matched state.
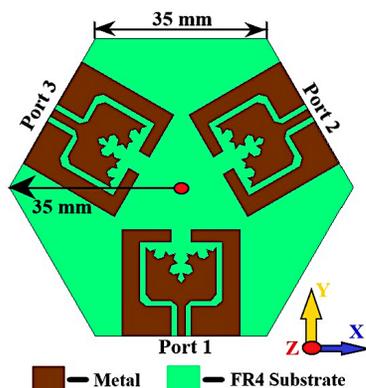

FIGURE 7. THPMIMOA layout.

ure 17 also shows an interesting phenomenon: the flows of currents on surfaces of adjacent antennas are in opposite directions. These opposing currents effectively neutralize the electromagnetic fields in the orthogonally located elements, thereby reducing mutual coupling. As a result, characteristic impedance of MIMO SEKCFA element changes, increasing the isolation between the elements. In addition, the current distribution pattern shows a countercurrent between the ground and radiating elements, which further improves the isolation by reducing current transfer to neighboring elements.

3. RESULTS AND DISCUSSION

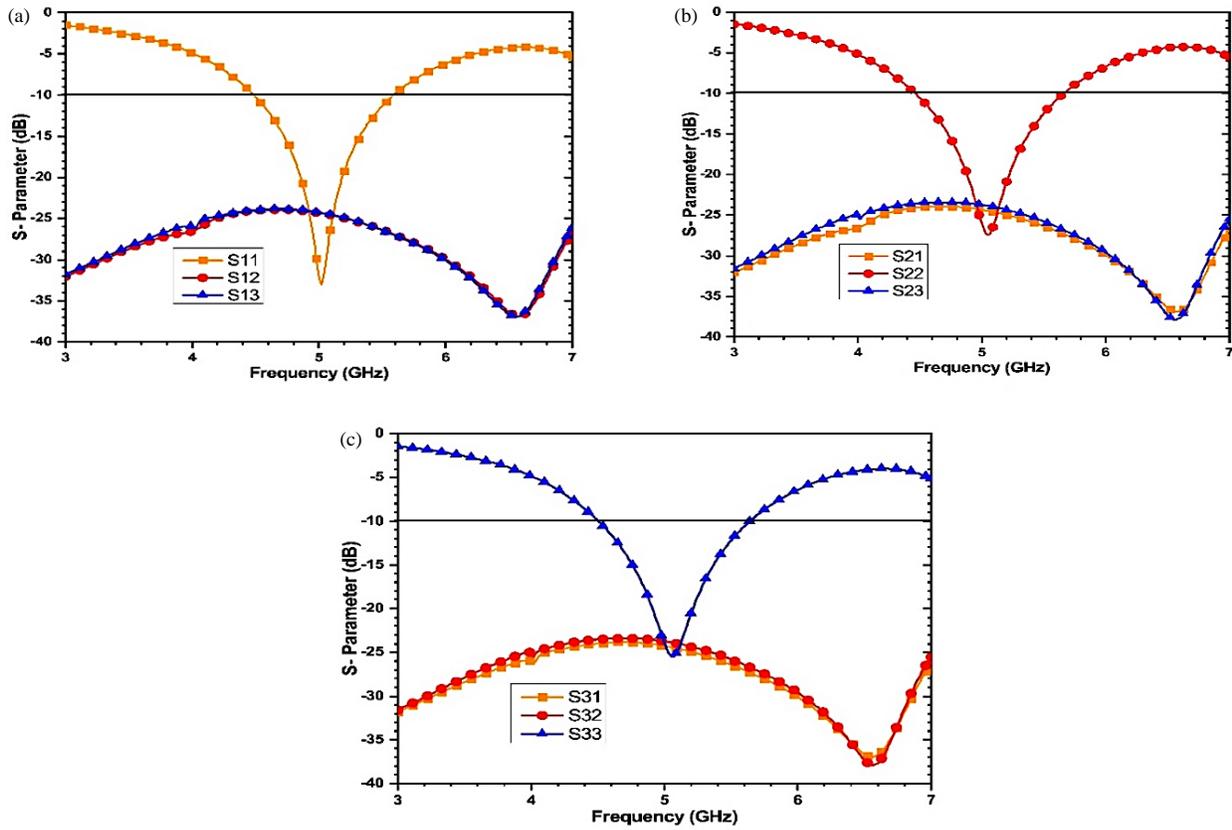From THMIMOA and FPMIMOA layouts, FPMIMOA is selected for prototyping as the results of FPMIMOA are better

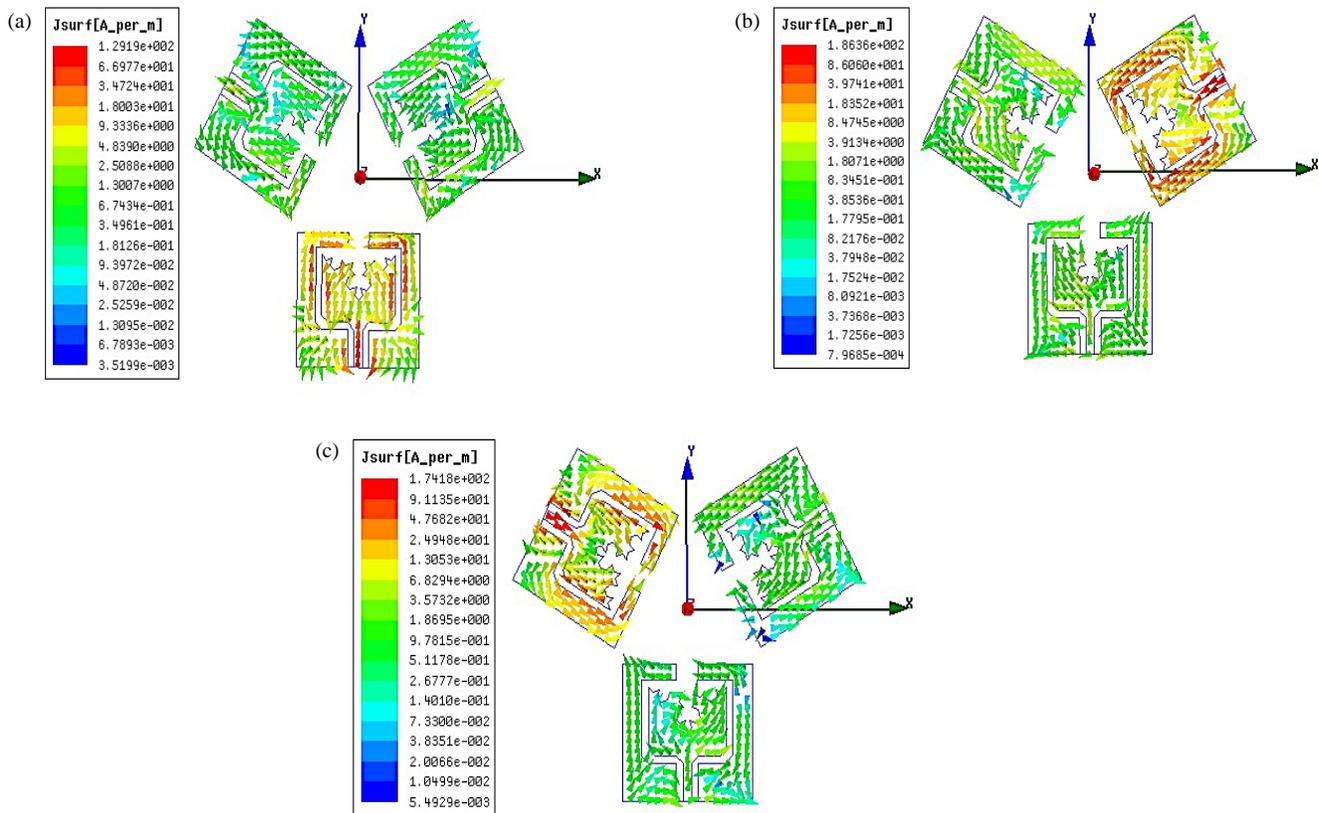**FIGURE 8**. S-P of THPMIMOA layout.

FIGURE 9. SC distributions over the antenna surface of THPMIMOA layout at 5 GHz when (a) Port 1 is excited, (b) Port 2 is excited, and (c) Port 3 is excited.
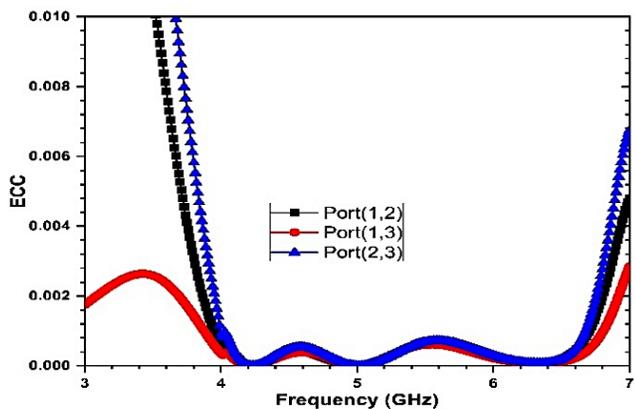
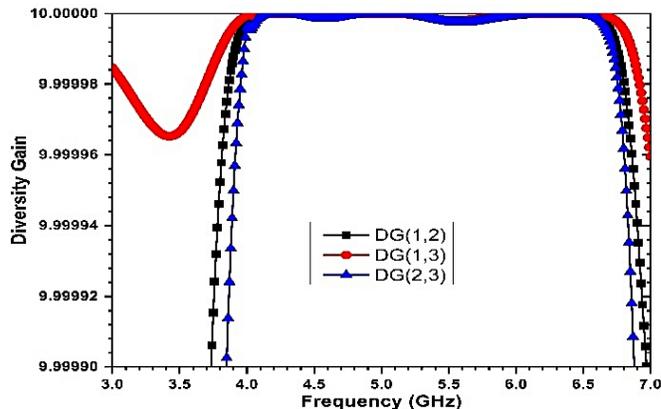FIGURE 10. ECC between the adjacent and diagonal ports for the THP-MIMOA.
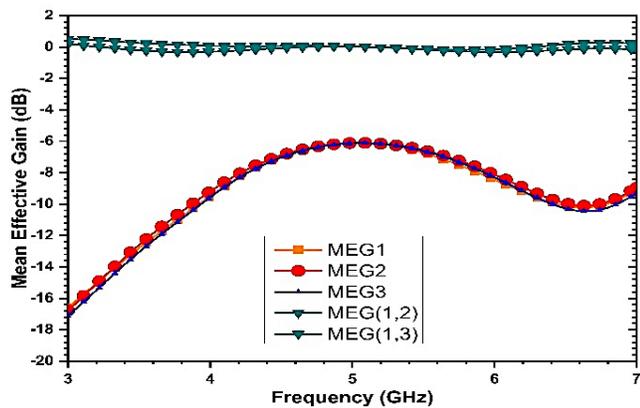

FIGURE 11. DG for the THPMIMOA.

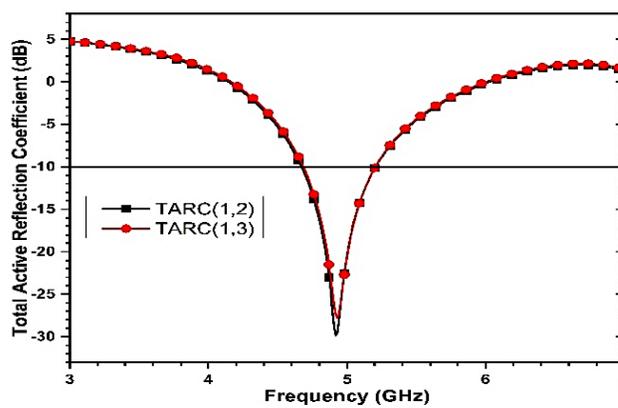
FIGURE 12. MEGs of the THPMIMOA for Ports 1, 2, and 3.

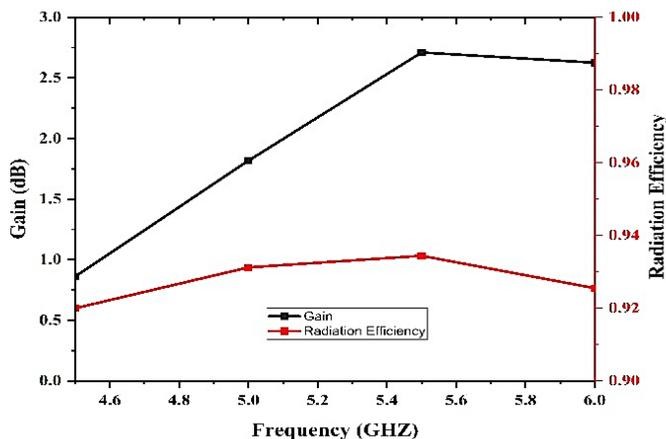FIGURE 13. TARC of the THPMIMOA.
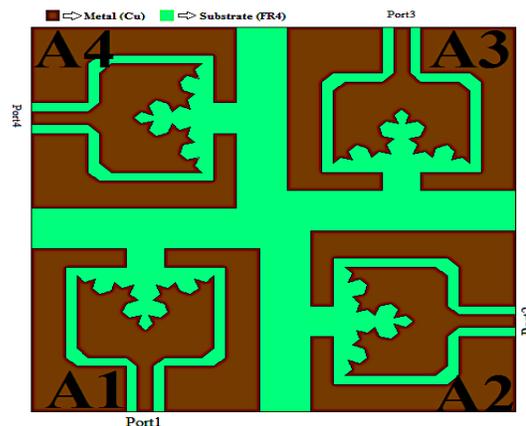

FIGURE 14. Gain and η plot of FPMIMOA.

FIGURE 15. FPMIMOA layout.

than THMIMOA, and also the overall size of FPMIMOA is smaller than THMIMOA. To verify circuit and radiation properties, the prototype of TPMIMOA, shown in Figure 18(a), is fabricated. The S-P and radiation performance are measured in lab using Vector Network Analyzer and in an anechoic chamber. These lab tests provide a thorough evaluation of circuit and radiation behavior of the FPMIMOA.

Figure 18(b) presents the measured and simulated S-P of FP-MIMOA across all four ports, with a particular emphasis on Port 1. Measured parameters closely align with the simulated results, though minor discrepancies are observed. These variations may arise due to copper loss, slight misalignment of connector and feed line, fabrication tolerances, and constraints of the laboratory. Minor discrepancies in the bandwidth can be seen in the simulated and measured results, but that does not affect the usability of FPMIMOA for the targeted application as it covers the required bandwidth. To see the practicality of the FPMIMO antenna, many diversity parameters are thoroughly
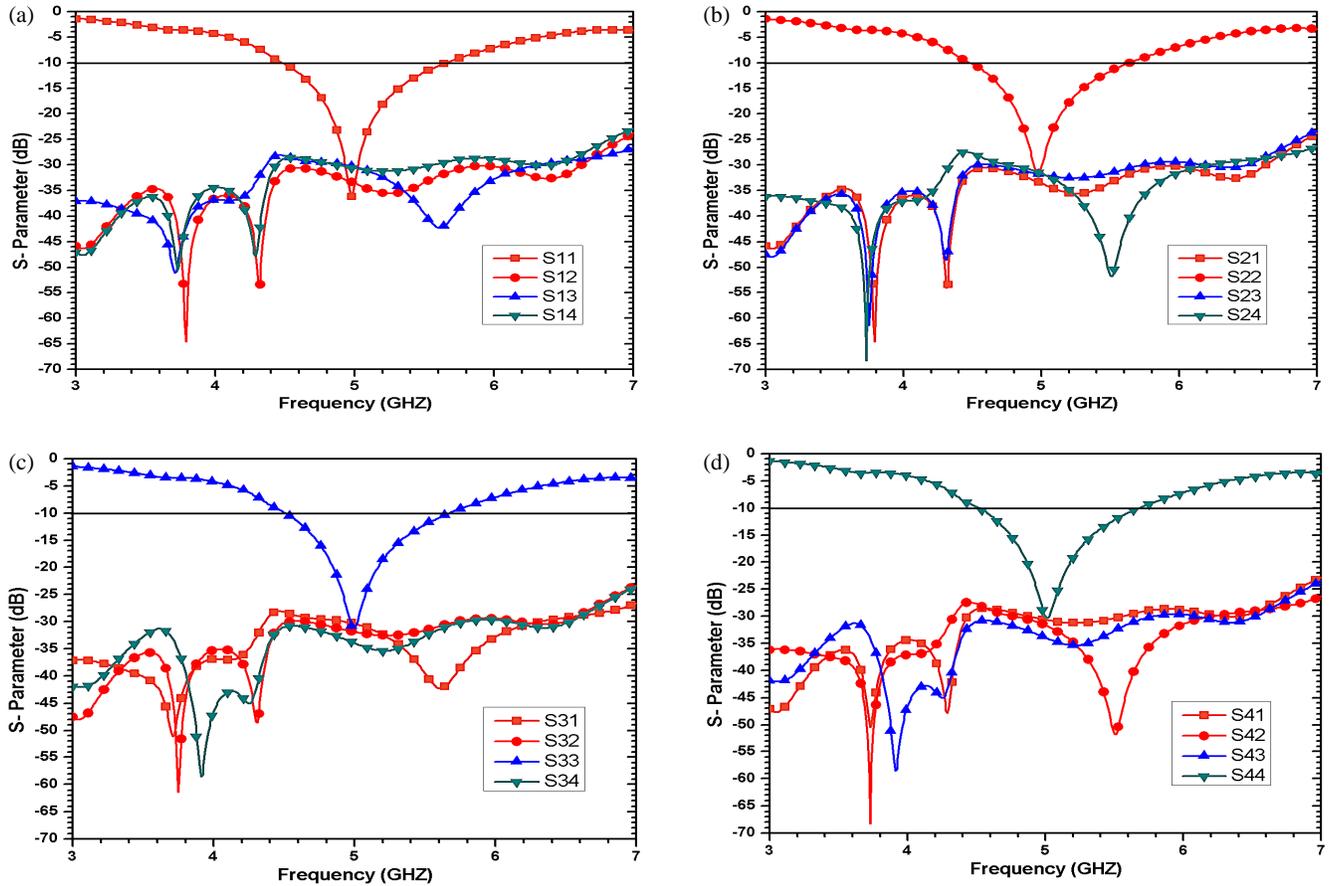
FIGURE 16. S-parameters of the FPMIMOA layout at (a) Port 1, (b) Port 2, (c) Port 3, (d) Port 4.

examined. These factors — such as mutual coupling, ECC, DG, CCL, and isolation — are crucial for determining the capability of systems. A broader understanding of the above stated parameters is a key to designing such systems with optimum functionality. The following discussion provides a detailed analysis of these aspects.

3.1. ECC

ECC quantifies the similarity between the radiation patterns of two antennas and helps assess the correlation between their received signal envelopes. A lower value of ECC shows reduced mutual coupling between the antennas. For optimal MIMOA performance, the ECC should be below 0.5.

It can be calculated using S-P and far field method [21–23, 31–33]. Equation (1) given below is used to calculate ECC from S-P:

$$\text{ECC} = \frac{\left| S_{pp}^* S_{pq} + S_{qp}^* S_{qq} \right|^2}{\left(1 - |S_{pp}|^2 - |S_{qp}|^2 \right) \left(1 - |S_{qq}|^2 - |S_{pq}|^2 \right)} \quad (1)$$

Equation (2) given below is used to calculate ECC from far field:

$$\text{ECC} =$$

$$\frac{\iint_{4\pi} E_p(\theta, \emptyset) \cdot E_q(\theta, \emptyset)\, d\Omega}{\sqrt{\iint_{4\pi} E_p(\theta, \emptyset) \cdot E_p^*(\theta, \emptyset)\, d\Omega_{4\pi} E_q(\theta, \emptyset) \cdot E_q^*(\theta, \emptyset)\, d\Omega}} \quad (2)$$

where E_p and E_q are far-field radiation patterns generated from ports p and q, respectively. ECC for the FPMIMOA is depicted in Figures 19(a)–(d) which has a value of less than 0.01 for the entire operating band. Figures 19(a) and (b) show the value calculated using S-P while images (c) and (d) show the ECC calculated using far field method which confirms that FPMIMOA has a good diversity performance.

3.2. DG

DG measures the improvement in signal quality achieved by using a number of antennas rather than a single one. The use of more than one antenna helps the system overcome issues like fading and interference, which can degrade the received signal. DG acts as an indicator of how much the signal quality improves due to multiple antennas, with an optimal value generally near 10 dB in operating region. A higher DG signifies better overall system performance. To compute DG, the ECC value is used in Equation (3) [14, 23, 32], as given below:

$$\text{DG} = 10 \times \sqrt{1 - |\text{ECC}|^2} \quad (3)$$

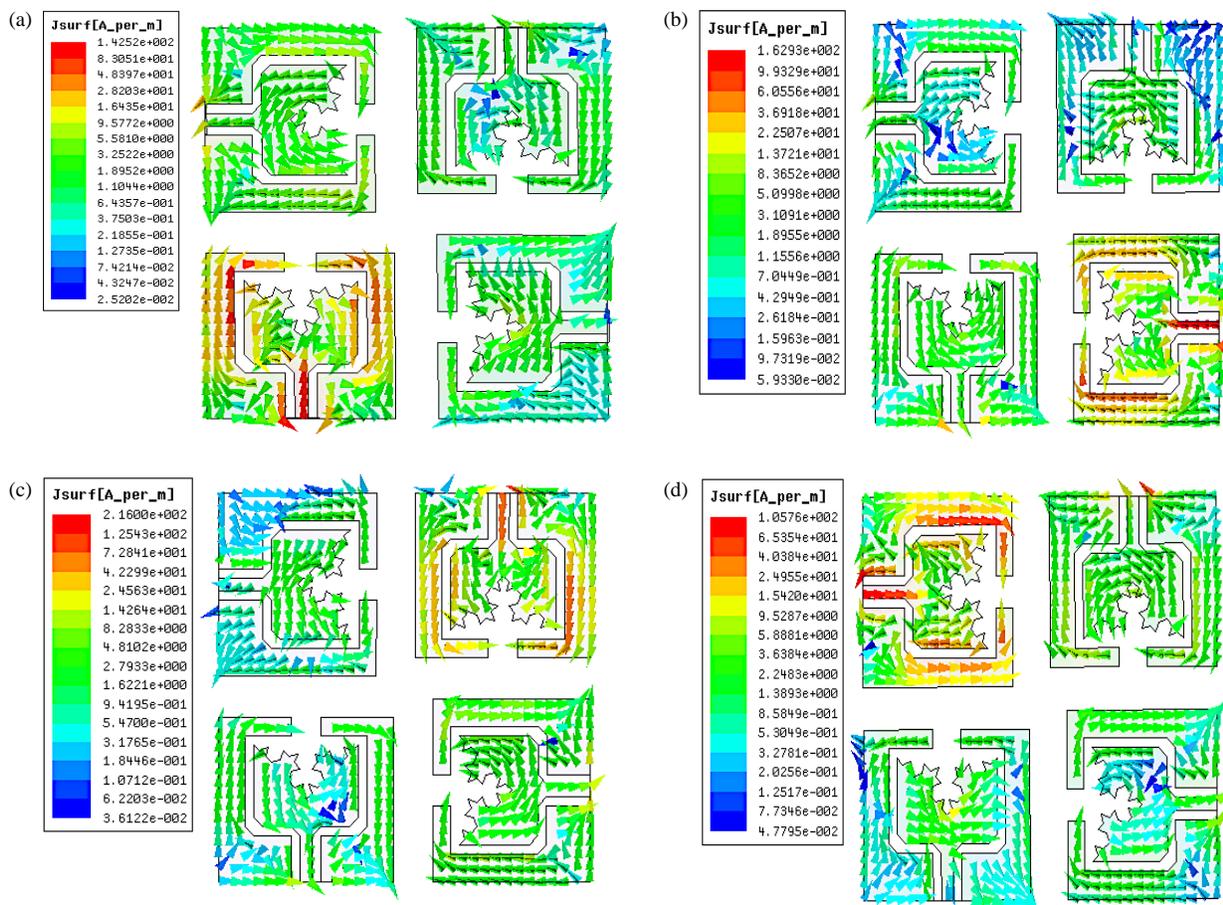DG for FPMIMOA is above 9.8 dB in operating region as shown in Figure 20.

FIGURE 17. FPMIMOA layout SC distribution at 4.9 GHz when (a) Port 1, (b) Port 2, (c) Port 3, and (d) Port 4 are excited, with the remaining ports in a matched state.
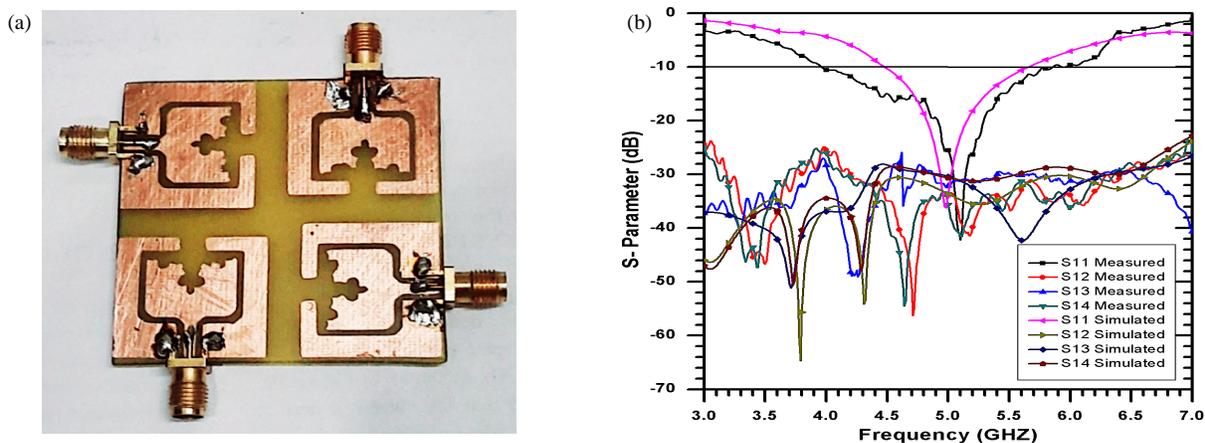

FIGURE 18. (a) Prototype of the FPMIMOA, and (b) FPMIMOA S-P comparisons between simulated and measured at Port 1.

3.3. MEG

MEG plays a vital role in designing and analyzing multiple antenna systems, providing valuable information about overall η, gain, and propagation effects in a multipath fading environment. For a MIMOA system, it should be under -3 dB. In the evaluation of the FPMIMOA system, MEG is analyzed across all four ports, as illustrated in Figure 21. MEG(m, n) is the ratio

of $MEGm$ to MEGn. MEG is computed using Equations (4) and (5) [14, 22, 23].

$$\text{MEG}m = 0.5 \times \left[1 - |S_{mm}|^2 - |S_{mn}|^2 \right] \tag{4}$$

$$\text{MEG}n = 0.5 \times \left[1 - |S_{mn}|^2 - |S_{nn}|^2 \right] \tag{5}$$
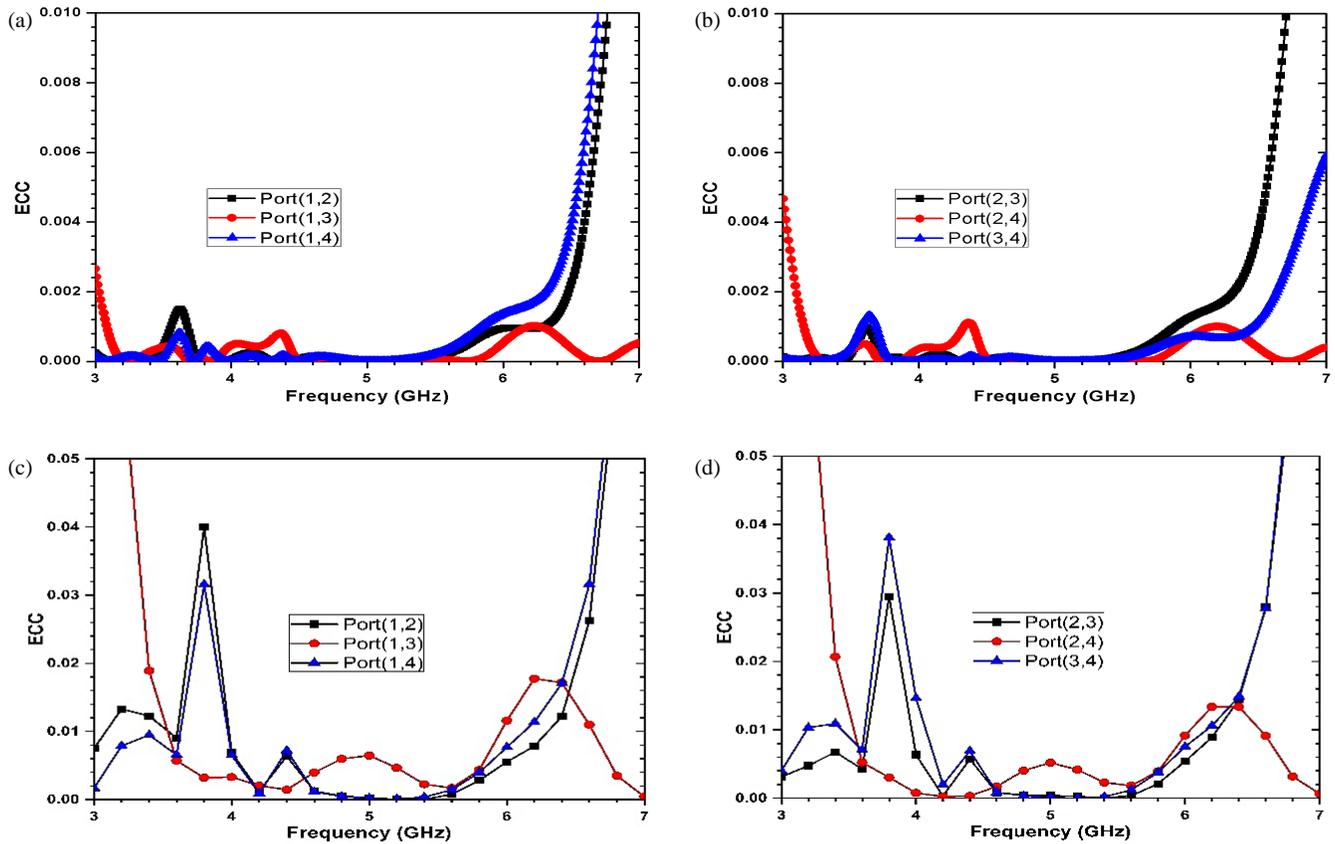
FIGURE 19. ECC between the adjacent and diagonal ports for the FPMIMOA, (a), (b) using S-P, and (c), (d) using far field.
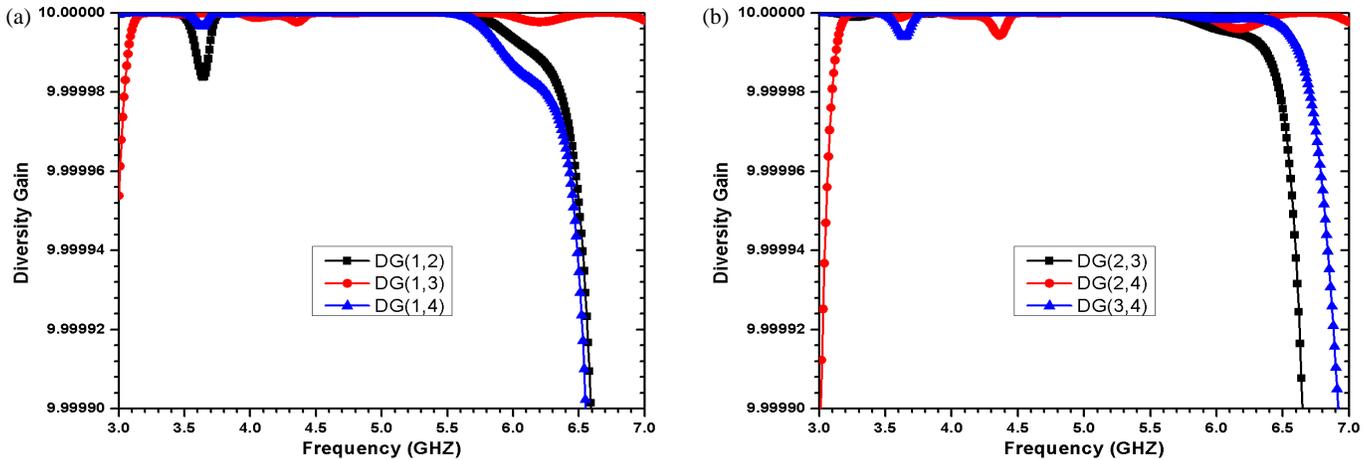

FIGURE 20. DG for the FPMIMOA.

3.4. TARC

It is square root of the ratio between the total power reflected to incident to all ports and also by using the S-P from Equations (6) and (7) [14, 23, 32].

$$\text{TARC} = \frac{\sqrt{\sum_{m=1}^{N} |R_m|^2}}{\sqrt{\sum_{m=1}^{N} |I_m|^2}} \quad (6)$$

$$\text{TARC} = \sqrt{\frac{\left|(S_{11} + S_{12}e^{j\theta})\right|^2 + \left|(S_{22} + S_{21}e^{j\theta})\right|^2}{2}} \quad (7)$$

In Equation (5), R_m is the reflected signal, and I_m is the incident signal. To achieve an efficient MIMOA system, the TARC value should remain under $-10\,\text{dB}$ in operating band. It can be observed from Figure 22 that the TARC values for Port 1 to Ports 2, 3, and 4 of the FPMIMOA are all under $-10\,\text{dB}$.

3.5. CCL

CCL measures the reduction in the highest possible data rate of a communication channel due to factors such as attenuation, noise, and interference. It indicates the decline in the ability of
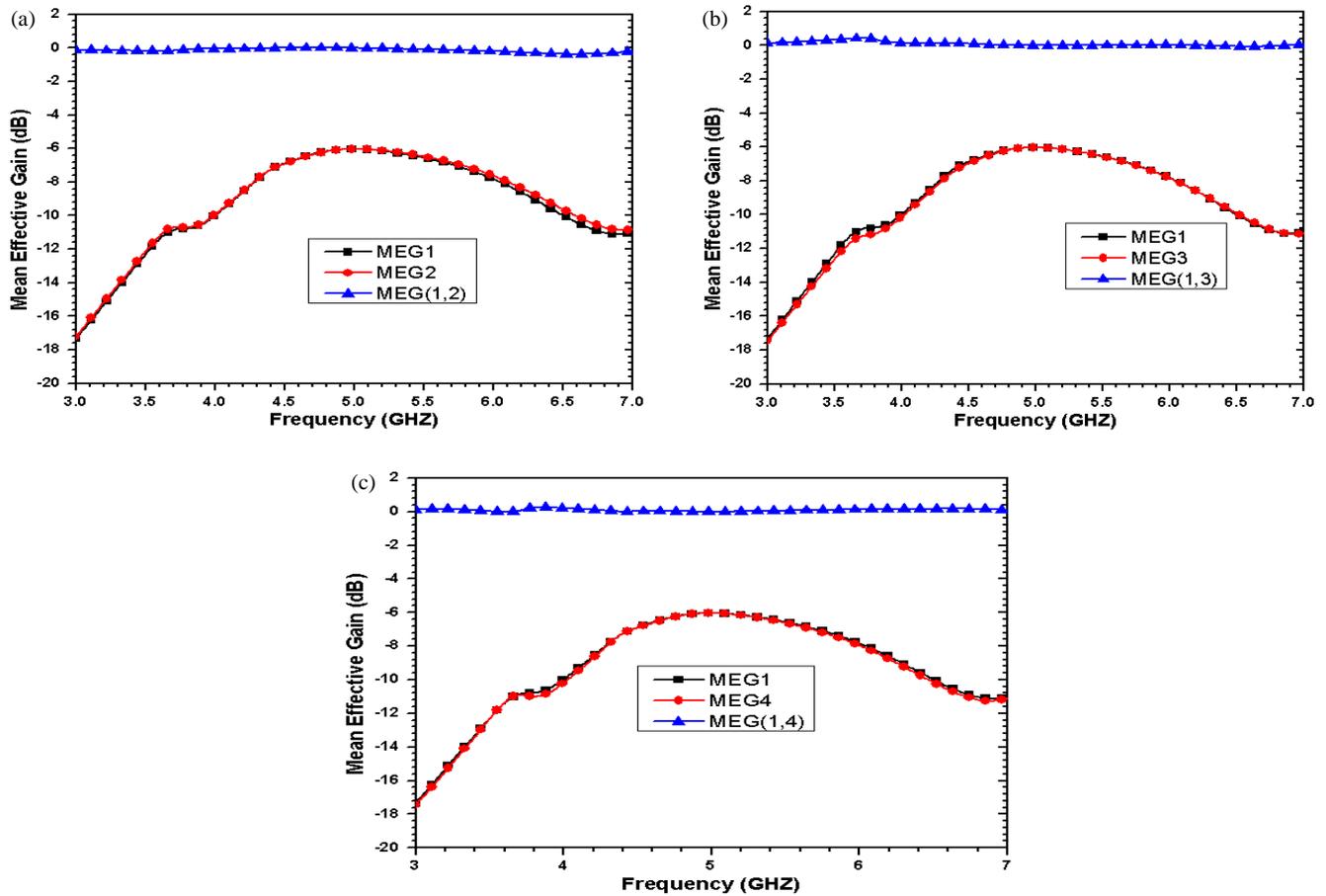
FIGURE 21. MEG of the FPMIMOA for (a) Ports 1 and 2, (b) Ports 1 and 3, and (c) Ports 1 and 4.

TABLE 1. Comparison with related work.

| Ref. No.	Size (λ^2)	Frequency Range (GHz)	Gain (dBi)	Isolation (dB)	EC-C	MEG (dB)	Fractal/ Non-fractal
[2]	0.792×0.792	3.3–6.0	2.5	15	0.005	-	Fractal
[27]	0.39×0.39	3.72–3.82, 4.65–4.76, 6.16–6.46	2.5	16	< 0.1	Ratio between 1–1.3 dB	Non-Fractal
[21]	1.7×0.85	3.4–3.6, 4.8–5	-	16.5	0.01	< -3	Non-Fractal
[34]	0.62×0.61	2.66–3.82, 4.57–4.91, 6.06–6.50, 7.53–8.08	4.19	24	< 0.4	< 3	Fractal
[8]	0.33×0.33	2.2–6.28	2.75	10.0	< 0.25	≈ -3	Non-Fractal
[35]	0.58×0.58	3.15–20	6.1	15	< 0.008	< -3	Fractal
[13]	0.72×0.72	4.3–6.65	4	20	< 0.004	-	Non-Fractal
[14]	0.6×0.6	4.3–6.8	4.95	> 20	< 0.2	< -3	Non-Fractal
[22]	0.3×0.3	1.55–2.65, 3.35–3.65	2.2, 3.8	> 10, > 19	< 0.08, < 0.02	-	Non-Fractal
[23]	2.2×1.72	5.15–5.925	4.85	15	0.05	≈ -6	Non-Fractal
[25]	1.08×1.08	5.025–5.135	2.7	36	< 0.003	-	Non-Fractal
[24]	2.98×1.31	5.6–5.67	-	30	0.06	-	Non-Fractal
[26]	1.25×1.36	3–5	4.85	20	< 0.2	-	Non-Fractal
Proposed work	0.75×0.75	4.46–5.69	3.14	> 28	< 0.004	≈ -6	Fractal
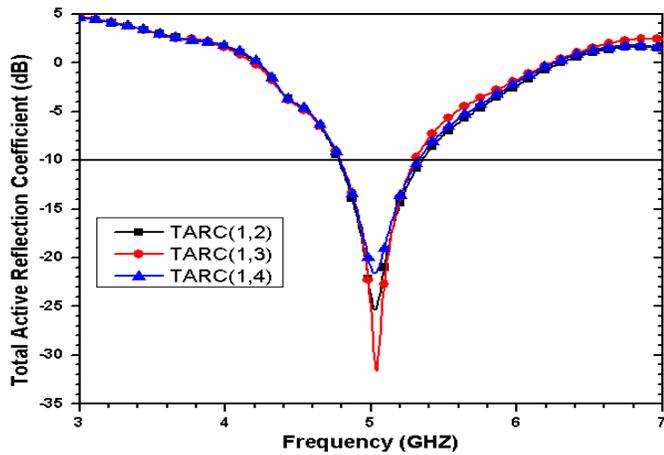
FIGURE 22. TARC of the FPMIMOA.
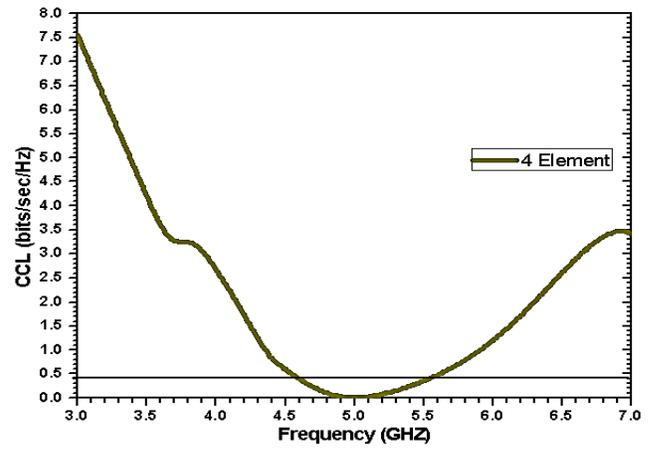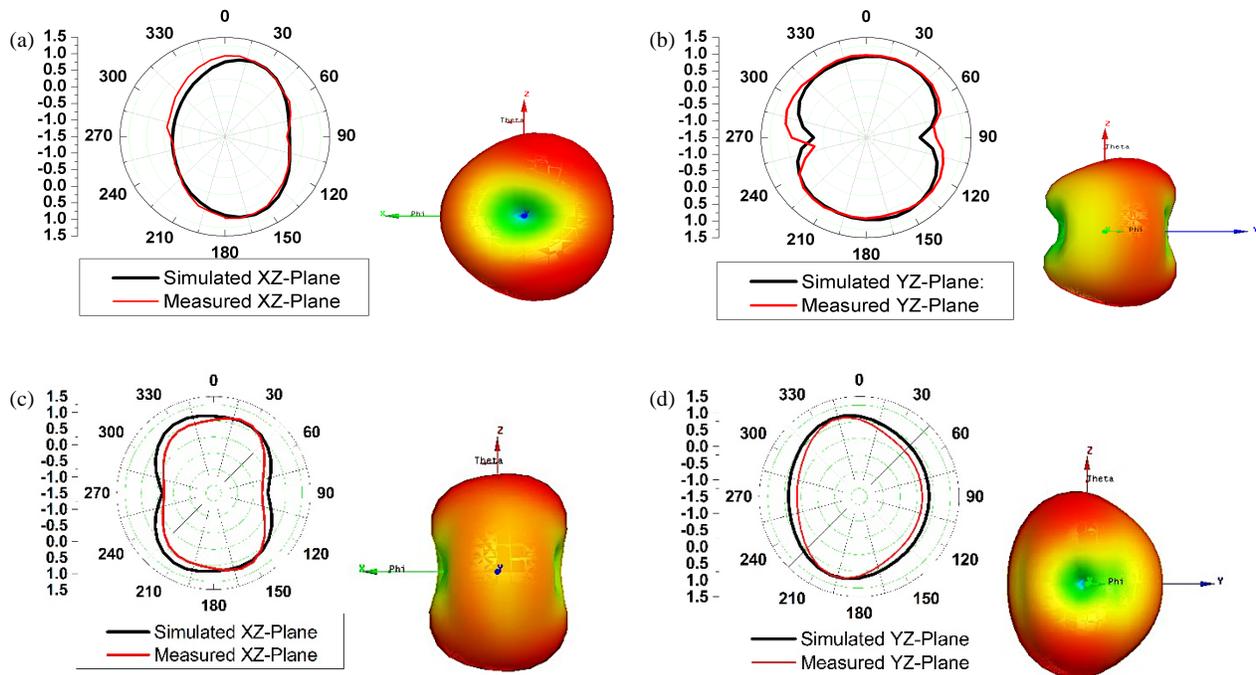

FIGURE 23. CCL of the FPMIMOA.

FIGURE 24. Radiation properties of the FPMIMOA, (a), (b) at 4.92 GHz, and (c), (d) at 5.2 GHz.

system to transmit data efficiently. Grasping the idea of CCL is essential to improving performance of system and maximizing η. For MIMOA systems, maintaining a CCL value below 0.4 bits/s/Hz is preferable. CCL calculation can be done using Equations (8)–(11) [22] based on the S-P. Figure 23 presents the calculated CCL values for the FPMIMOA, showing that they remain well below the designated limit of 0.4 bits/s/Hz.

$$\text{CCL} = -\log_2 \left| c^R \right| \tag{8}$$

$$c^R = \begin{bmatrix} c_{11} & c_{12} & c_{13} & c_{14} \\ c_{21} & c_{22} & c_{23} & c_{24} \\ c_{31} & c_{32} & c_{33} & c_{34} \\ c_{41} & c_{42} & c_{43} & c_{44} \end{bmatrix} \tag{9}$$

$$c_{ii} = 1 - \left| \sum_{n=1}^{N} S_{in}^* S_{ni} \right| \quad \text{for } i, j = 1, 2, 3 \text{ and } 4 \tag{10}$$

$$c_{ij} = - \left| \sum_{n=1}^{N} S_{in}^* S_{nj} \right| \tag{11}$$

3.6. Radiation Properties

The radiation properties of the FPMIMOA are confirmed through measurements done in an anechoic chamber, ensuring alignment with the simulated results. Figure 24 presents the normalized simulated and measured radiation properties in the XZ-plane and YZ-plane, along with 3D-Polar plots

at 4.92 GHz and 5.2 GHz. The radiation in the YZ-plane demonstrates bidirectional behavior, whereas in the XZ-plane, the FPMIMOA radiates almost uniformly in every direction.

3.7. Gain and Radiation Efficiency (η)

Figure 25 presents simulated gain and η plot of FPMIMOA. It is noted that the maximum gain within the operating range reaches approximately 3.2 dBi at 4.92 GHz. Additionally, the η remains above 90% throughout the operating region. Comparison between the FPMIMOA and previous studies from the literature is tabulated in Table 1. The data clearly indicate that the FPMIMOA outperforms its counterparts in terms of performance.
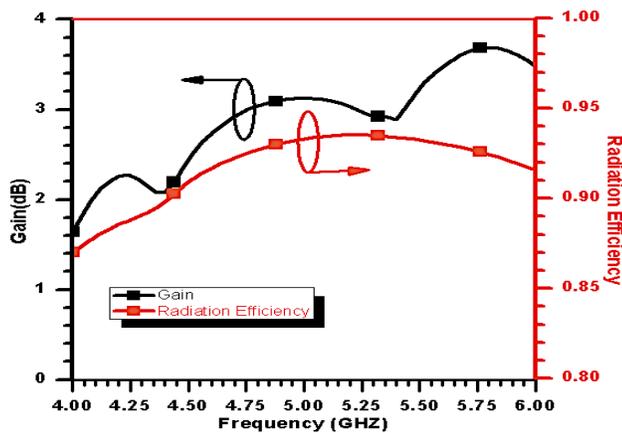

FIGURE 25. Gain and η plot of FPMIMOA.

4. CONCLUSION

A CPW-fed four-port MIMO antenna (FPMIMOA) integrating a symmetrically etched Koch curve fractal antenna (SEKCFA) has been designed, offering an impedance bandwidth of 1230 MHz (4.46–5.69 GHz). The antenna's performance has been thoroughly analyzed, revealing a high isolation level exceeding 28 dB without the use of any dedicated isolation techniques. To minimize coupling between the radiating elements, key parameters such as Total Active Reflection Coefficient (TARC), Envelope Correlation Coefficient (ECC), Channel Capacity Loss (CCL), Mean Effective Gain (MEG), and Diversity Gain (DG) have been meticulously evaluated. This FPMIMOA is suitable for multiple applications, including public safety communications, 4800–5000 MHz band within the 5G sub-6 GHz spectrum, and 5.2 GHz Wireless LAN band (5.15–5.35 GHz). The outstanding performance of the proposed MIMKOA design demonstrates significant potential for the aforementioned applications.

ACKNOWLEDGEMENT

REFERENCES

[1] Kumar, A., A. Kumar, and A. J. A. Al-Gburi, "Development of semi-circular corner cut MIMO antenna for 5G-advanced and 6G automotive wireless applications," *Results in Engineering*, Vol. 25, 103805, Mar. 2025.

[2] Kumar, A., G. Singh, M. K. Abdulhameed, S. R. Hashim, and A. J. A. Al-Gburi, "Development of fractal 5G MIMO antenna for sub 6 GHz wireless automotive applications," *Progress In Electromagnetics Research M*, Vol. 130, 121–128, 2024.

[3] Jemaludin, N., A. J. A. Al-Gburi, R. H. Elabd, T. Saeidi, M. F. Akbar, I. M. Ibrahim, and Z. Zakaria, "A comprehensive review on MIMO antennas for 5G smartphones: Mutual coupling techniques, comparative studies, SAR analysis, and future directions," *Results in Engineering*, Vol. 23, 102712, 2024.

[4] Elabd, R. H. and A. J. A. Al-Gburi, "Low mutual coupling miniaturized dual-band quad-port MIMO antenna array using decoupling structure for 5G smartphones," *Discover Applied Sciences*, Vol. 6, No. 4, 189, 2024.

[5] Kumar, P., A. K. Singh, R. Kumar, S. K. Mahto, P. Pal, R. Sinha, A. Choubey, and A. J. A. Al-Gburi, "Design and analysis of low profile stepped feedline with dual circular patch MIMO antenna and stub loaded partial ground plane for wireless applications," *Progress In Electromagnetics Research C*, Vol. 140, 135–144, 2024.

[6] Kumar, P. S. and B. C. Mohan, "Design of a compact two element MIMO antenna with improved bandwidth and isolation," in *2015 International Conference on Microwave, Optical and Communication Engineering (ICMOCE)*, 389–392, Bhubaneswar, India, Dec. 2015.

[7] Sohi, A. K. and A. Kaur, "Slot and SRR-loaded quad-port, hen-shaped fractal UWB-MIMO antenna with quad band-reject ability for handheld 4G/5G wireless devices," *Iranian Journal of Science and Technology, Transactions of Electrical Engineering*, Vol. 47, No. 3, 1187–1205, Mar. 2023.

[8] Anitha, R., P. V. Vinesh, K. C. Prakash, P. Mohanan, and K. Vasudevan, "A compact quad element slotted ground wideband antenna for MIMO applications," *IEEE Transactions on Antennas and Propagation*, Vol. 64, No. 10, 4550–4553, 2016.

[9] Barani, I. R. R. and K.-L. Wong, "Integrated inverted-F and open-slot antennas in the metal-framed smartphone for 2×2 LTE LB and 4×4 LTE M/HB MIMO operations," *IEEE Transactions on Antennas and Propagation*, Vol. 66, No. 10, 5004–5012, 2018.

[10] Sarkar, D., K. Saurav, and K. V. Srivastava, "A compact dual band four element MIMO antenna for pattern diversity applications," in *2016 IEEE 5th Asia-Pacific Conference on Antennas and Propagation (APCAP)*, 273–274, Kaohsiung, Taiwan, Jul. 2016.

[11] Rosaline, I., A. Kumar, P. Upadhyay, and A. H. Murshed, "Four element MIMO antenna systems with decoupling lines for high-speed 5G wireless data communication," *International Journal of Antennas and Propagation*, Vol. 2022, No. 1, 9078929, Jun. 2022.

[12] Kumar, A., V. Prakash, S. C. Padhy, *et al.*, "Four port MIMO antenna for IoT applications in public safety band and sub-6 GHz TDD 5G band," *Engineering Research Express*, Vol. 6, No. 1, 015309, 2024.

[13] Elabd, R. H. and A. J. A. Al-Gburi, "Super-compact 28/38 GHz 4-port MIMO antenna using metamaterial-inspired EBG structure with SAR analysis for 5G cellular devices," *Journal of Infrared, Millimeter, and Terahertz Waves*, Vol. 45, No. 1, 35–65, 2024.

[14] Al Gburi, A. J. A., "5G MIMO antenna: Compact design at 28/38 GHz with metamaterial and SAR analysis for mobile phones," *Przegląd Elektrotechniczny*, Vol. 2024, No. 4, 171–174, 2024.

[15] Bai, J., R. Zhi, W. Wu, M. Shangguan, B. Wei, and G. Liu, "A novel multiband MIMO antenna for TD-LTE and WLAN applications," *Progress In Electromagnetics Research Letters*, Vol. 74, 131–136, 2018.

[16] Mistri, R. K., S. K. Mahto, A. K. Singh, R. Sinha, A. J. A. Al-Gburi, T. A. H. Alghamdi, and M. Alathbah, "Quad element MIMO antenna for C, X, Ku, and Ka-band applications," *Sensors*, Vol. 23, No. 20, 8563, 2023.

[17] Ali, A., M. E. Munir, M. Marey, H. Mostafa, Z. Zakaria, A. J. A. Al-Gburi, and F. A. Bhatti, "A compact MIMO multiband antenna for 5G/WLAN/WIFI-6 devices," *Micromachines*, Vol. 14, No. 6, 1153, 2023.

[18] Sun, L., Y. Li, Z. Zhang, and H. Wang, "Self-decoupled MIMO antenna pair with shared radiator for 5G smartphones," *IEEE Transactions on Antennas and Propagation*, Vol. 68, No. 5, 3423–3432, May 2020.

[19] Xing, H., X. Wang, Z. Gao, X. An, H.-x. Zheng, M. Wang, and E. Li, "Efficient isolation of an MIMO antenna using defected ground structure," *Electronics*, Vol. 9, No. 8, 1265, 2020.

[20] Iqbal, A., O. A. Saraereh, A. Bouazizi, and A. Basir, "Metamaterial-based highly isolated MIMO antenna for portable wireless applications," *Electronics*, Vol. 7, No. 10, 267, Oct. 2018.

[21] Huang, J., G. Dong, J. Cai, H. Li, and G. Liu, "A quad-port dual-band MIMO antenna array for 5G smartphone applications," *Electronics*, Vol. 10, No. 5, 542, Feb. 2021.

[22] Abdulkawi, W. M., W. A. Malik, S. U. Rehman, A. Aziz, A. F. A. Sheta, and M. A. Alkanhal, "Design of a compact dual-band MIMO antenna system with high-diversity gain performance in both frequency bands," *Micromachines*, Vol. 12, No. 4, 383, 2021.

[23] He, Z. and J. Jin, "Compact quad-port MIMO antenna with ultra-wideband and high isolation," *Electronics*, Vol. 11, No. 20, 3408, Oct. 2022.

[24] Khan, J., S. Ullah, F. A. Tahir, F. Tubbal, and R. Raad, "A sub-6 GHz MIMO antenna array for 5G wireless terminals," *Electronics*, Vol. 10, No. 24, 3062, Dec. 2021.

[25] Wu, T., M.-J. Wang, and J. Chen, "Decoupling of MIMO antenna array based on half-mode substrate integrated waveguide with neutralization lines," *AEU — International Journal of Electronics and Communications*, Vol. 157, 154416, Dec. 2022.

[26] Thangarasu, D., S. K. Palaniswamy, and R. R. Thipparaju, "Quad port multipolarized reconfigurable MIMO antenna for sub 6 GHz applications," *International Journal of Antennas and Propagation*, Vol. 2023, No. 1, 8882866, Mar. 2023.

[27] Krishnamoorthy, R., A. Desai, R. Patel, and A. Grover, "4 element compact triple band MIMO antenna for sub-6 GHz 5G wireless applications," *Wireless Networks*, Vol. 27, No. 6, 3747–3759, 2021.

[28] Kumar, A., B. Dewan, A. Khandelwal, and K. Shrivastava, "On the devolvement of fractal antenna for IoT applications," *Engineering Research Express*, Vol. 5, No. 3, 035026, 2023.

[29] Kumar, A. and A. P. S. Pharwaha, "CPW-fed wide band micro-machined fractal antenna with band-notched function," *Applied Computational Electromagnetics Society Journal (ACES)*, Vol. 35, No. 8, 929–935, 2020.

[30] Kumar, A., A. Kumar, and A. P. S. Pharwaha, "On the development of super-wideband Sierpinski triangular fractal antenna," *Wireless Personal Communications*, Vol. 134, No. 1, 119–131, 2024.

[31] Cornelius, R., A. Narbudowicz, M. J. Ammann, and D. Heberling, "Calculating the envelope correlation coefficient directly from spherical modes spectrum," in *2017 11th European Conference on Antennas and Propagation (EUCAP)*, 3003–3006, Paris, France, Mar. 2017.

[32] El Hadri, D., A. Zakriti, A. Zugari, M. E. Ouahabi, and J. E. Aoufi, "High isolation and ideal correlation using spatial diversity in a compact MIMO antenna for fifth-generation applications," *International Journal of Antennas and Propagation*, Vol. 2020, No. 1, 2740920, 2020.

[33] Sharma, P., R. N. Tiwari, P. Singh, P. Kumar, and B. K. Kanaujia, "MIMO antennas: Design approaches, techniques and applications," *Sensors*, Vol. 22, No. 20, 7813, Oct. 2022.

[34] Anand, S. and A. Kumar, "Development of two port multilayer MIMO fractal antenna for multiband applications," *Engineering Research Express*, Vol. 7, No. 1, 015369, Mar. 2025.

[35] Kamal, M. M., B. Wang, N. Shoaib, U. Rafique, M. I. Abbasi, and M. R. Kamarudin, "Self-decoupled quad-port CPW-fed fractal MIMO antenna with UWB characteristics," *International Journal of Antennas and Propagation*, Vol. 2024, No. 1, 3826899, 2024.